New Journal of Physics
The open-access journal for physics

Time-resolved ion spectrometry on xenon with the jitter-compensated soft x-ray pulses of a free-electron laser

Maria Krikunova[1,5], Theophilos Maltezopoulos[1], Armin Azima[1], Moritz Schlie[1], Ulrike Frühling[2], Harald Redlin[2], Roland Kalms[1], Stefan Cunovic[3], Nikolay M Kabachnik[1,4], Marek Wieland[1] and Markus Drescher[1]

[1] Institut für Experimentalphysik, University of Hamburg, Luruper Chaussee 149, 22761 Hamburg, Germany
[2] HASYLAB at DESY, Notkestrasse 85, 22607 Hamburg, Germany
[3] Department of Physics, Bielefeld University, Universitätsstrasse 25, 33615 Bielefeld, Germany
[4] Institute of Nuclear Physics, Moscow State University, Moscow 119991, Russia
E-mail: maria.krikunova@desy.de

New Journal of Physics **11** (2009) 123019 (13pp)
Received 14 September 2009
Published 16 December 2009
Online at http://www.njp.org/
doi:10.1088/1367-2630/11/12/123019

Abstract. Atomic inner-shell relaxation dynamics were measured at the free-electron laser in Hamburg, FLASH, delivering 92 eV pulses. The decay of 4d core holes created in xenon was followed by detection of ion charge states after illumination with delayed 400 nm laser pulses. A timing jitter of the order of several hundred femtoseconds between laser- and accelerator-pulses was compensated for by a simultaneous delay measurement in a single-shot x-ray/laser cross-correlator. After sorting of the tagged spectra according to the measured delays, a temporal resolution equivalent to the pulse duration of the optical laser could be established. While results on ion charge states up to Xe^{4+} are compatible with a previous study using a high-harmonic soft x-ray source, a new relaxation pathway is opened by the nonlinear excitation of xenon atoms in the intense free-electron laser light field, leading to the formation of Xe^{5+}.

[5] Author to whom any correspondence should be addressed.

Contents

1. Introduction

The high photon energies of (hard or soft) x-rays enable them to penetrate deeply into the atomic electron shell, thereby delivering detailed information about the electronic structure. If the radiation is pulsed, the dynamical interplay of electrons during the relaxation of highly excited states becomes accessible [1]–[3]. Light pulses with wavelengths in the ultraviolet to visible range, on the other hand, act on loosely bound valence or Rydberg electrons, which may then initiate secondary processes, e.g. electron transfer, dissociation or isomerization in molecules. Consequently, utilizing a visible-pump/x-ray probe or x-ray-pump/visible-probe techniques, a wealth of ultrafast dynamical processes in atoms and molecules can be studied.

The new generation of accelerator-based free-electron lasers (FELs) for the soft x-ray (FLASH [4], FERMI [5]) and hard x-ray ranges (LCLS [6], SCSS [7], the European XFEL [8]) is therefore designed to deliver synchronized femtosecond (fs) light pulses from an external laser. In spite of a convincing performance in terms of pulse energy, energy range and tuneability, the applicability for visible/x-ray correlation experiments is limited by the degree of synchronization that can technically be realized. Previous studies at FLASH [9]–[11] indicate a residual laser/x-ray jitter of the order of 250 fs root mean square (rms). In spite of x-ray pulse durations of a few tens of fs [12, 13] pump–probe experiments performed in the usual manner by averaging data for each setting of a scanned optical delay line will therefore be limited in resolution to about 600 fs full-width-at-half-maximum (FWHM). Approaches that have been seriously investigated in order to overcome this jitter problem include improved synchronization schemes [14], seeding of the FEL's undulator with laser-generated radiation [15, 16] and generating short as well as long wavelengths in two serial undulators traversed by the same bunch of accelerated electrons [17].

As long as a solution for a highly synchronized visible and soft x-ray combination is not available, an alternative approach can be followed where the relative timing between laser and x-ray pulses is measured on a shot-to-shot basis, so that the tagged data of a simultaneously performed experiment can be sorted accordingly. This concept has proven its feasibility in time-resolved x-ray diffraction studies at the sub-picosecond pulse source (SPPS) at the Stanford

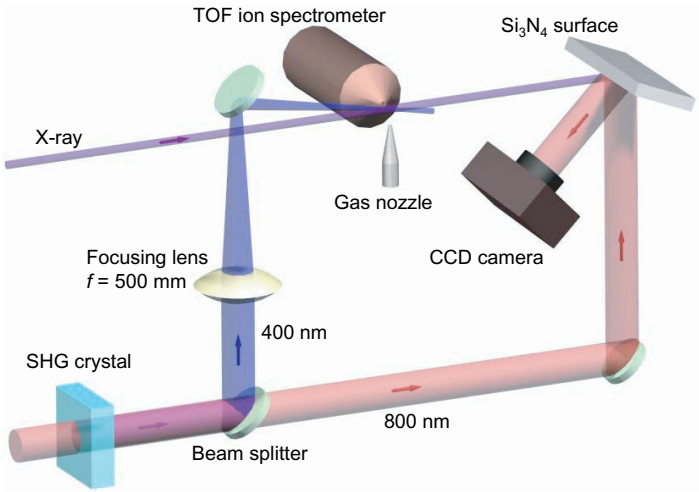

Figure 1. Scheme of the experimental geometry: x-ray and 400 nm pulses are overlapped at a small angle in an Xe gas target. Ions created in the interaction region are measured by a TOF ion mass spectrometer. A cross-correlator setup is installed behind the pump–probe experiment. The x-ray-induced reflectivity changes for the 800 nm light are imaged on to a CCD camera.

Linear Accelerator Center (SLAC) [18], where the timing information was deduced from electro-optical sampling (EOS) [19] of the relativistic electron bunches.

In a previous work we introduced a single-shot cross-correlator that directly compares the arrival times of visible and soft x-ray pulses at the experimental end-station of FLASH [20], thus removing timing uncertainties connected with the x-ray generation and the beam transport from the undulator to the experiment. In this work we present soft x-ray-pump/visible-probe experiments that demonstrate the degree of improvement achieved with this tagging concept. Relaxation dynamics following inner-shell excitation of atoms often occurs on a timescale of a few fs to a few tens of fs. As the system to be investigated initially, we have selected 4d core–hole creation in xenon (Xe) atoms, because the subsequent Auger decay has already been studied with sub-femtosecond temporal resolution using ionizing pulses from a laser-based high harmonic generation source [2]. Precise knowledge of the very short Xe-NOO Auger decay time constant (6.0 ± 0.7 fs) allows us to determine the achievable resolution with high precision. While in this case atomic dynamics mainly serves as a standard for an assessment of the achieved jitter compensation, use of very intense soft x-ray pulses from FLASH yields evidence of a decay channel not previously observed. Let us attribute its nonlinear behavior to a two-photon excitation of a core electron shell. Furthermore, with an ultrafast dynamical process as a reference, a direct comparison between the laser/x-ray cross-correlation and the EOS technique is possible, thereby contributing to the question as to whether a measurement of the electron timing can substitute for an all-optical cross-correlation.

2. Experimental setup

A scheme of the experimental geometry is shown in figure 1; the cross-correlator set-up is installed behind the pump–probe chamber, thus both experiments share the same x-ray beam. The experiment is performed at beamline BL1 of the FLASH facility operating at a photon

energy near 92 eV (13.4 nm wavelength), at a 5 Hz repetition rate in a single-bunch mode. The nominal x-ray focus position is between the pump–probe experiment and the x-ray/visible cross-correlator. A mode-locked Ti:sapphire laser system (800 nm, 120 fs FWHM, pulse energy 2 mJ), provided by the FLASH facility, is electronically synchronized with the 1.3 GHz master clock. The 800 nm pulses are frequency doubled in a 350 μm thick BBO crystal to 400 nm and 300 μJ pulse energy. A beam splitter reflects the 400 nm beam to the pump–probe experiment, while the x-ray/optical cross-correlator is operated with the remaining 800 nm light.

In the interaction region of the pump–probe experiment, the 400 nm probing laser pulse is focused to a 40 μm FWHM spot size with an estimated average intensity of 2×10^{14} W cm^{-2}. For the x-ray pump pulse an average target intensity of the order of 8×10^{11} W cm^{-2} is estimated by assuming 35 fs FWHM pulse duration [12] and a spot size of about 150 μm FWHM. The x-ray and laser beams overlap at an angle of $\sim 2^{\circ}$ in an Xe gas target, thus keeping the blurring of the temporal overlap between pump and probe pulses below 17 fs. The pressure in the pump–probe chamber with and without target gas was $\sim 10^{-6}$ and $\sim 10^{-7}$ mbar, respectively. Different charge states of Xe ions created in the target volume are detected by a time-of-flight (TOF) ion mass-to-charge spectrometer. Scans with different visible laser intensity at the target reveal that the Xe^{2+} ion yield is almost solely determined by the x-ray pulse intensity. Within the evaluated range of intensities, it shows linear dependence on the x-ray pulse energy measured by the gas-monitor detector in the FLASH tunnel [4]. Thus, single-ion spectra are normalized to the ion yield of Xe^{2+} to compensate for shot-to-shot intensity fluctuations of the x-ray pulses. Temporal prealignment between x-ray and laser pulses is accomplished with ± 10 ps accuracy using a high bandwidth copper photocathode [9]. The arrival time of the optical laser with respect to the x-ray pulse can be scanned within a several nanoseconds (ns) time window from negative values (optical probe first) to positive values (x-ray pump first) by an optical delay line available at FLASH. According to the mathematical model used [2] the inflection point of the Xe^{3+} transient profile corresponds to the coincidence of the peaks of the x-ray and laser pulses. Before the cross-correlator setup, another delay stage for the visible beam compensates for the optical pathway difference between both experiments.

A detailed description of the x-ray/visible cross-correlator can be found in [20]. Briefly, the x-ray and the visible pulse are non-collinearly overlapped in space and time on an Si_3N_4 surface. Along its path, the x-ray pulse changes the reflectivity of the sample for the optical pulse, which is imaged on to a CCD array. The spatial position of the reflectivity change determines the individual x-ray arrival time. Due to a longer damage-free lifetime, an Si_3N_4 instead of a GaAs [20] wafer was used in the current study. A typical single-shot image of the reflectivity change on Si_3N_4 is shown in figure 2(a), where the space-coordinate is already converted into a time-coordinate by geometrical considerations. This area, where the FEL pulse has excited the Si_3N_4 sample prior to the arrival of the optical pulse, appears brighter. Note that the x-ray pulse induces a reflectivity enhancement for 800 nm on Si_3N_4, instead of a reflectivity decrease as observed for GaAs. To improve the image quality, the 800 nm light passes through a spatial frequency filter before hitting the substrate. CCD raw images were background subtracted and filtered in order to correct for the remaining interference fringes and inhomogeneous illumination. An average of horizontal signal pixels within the region of interest (ROI) marked in figure 2(a) is shown in figure 2(b). The slope width of the rising edge of about 110 fs is in good agreement with the laser pulse duration of 120 fs. The inflection point is further used as an arrival-time marker for the x-ray pulse. Changes of one pixel on the CCD chip correspond to 17 fs changes of the x-ray relative arrival time.

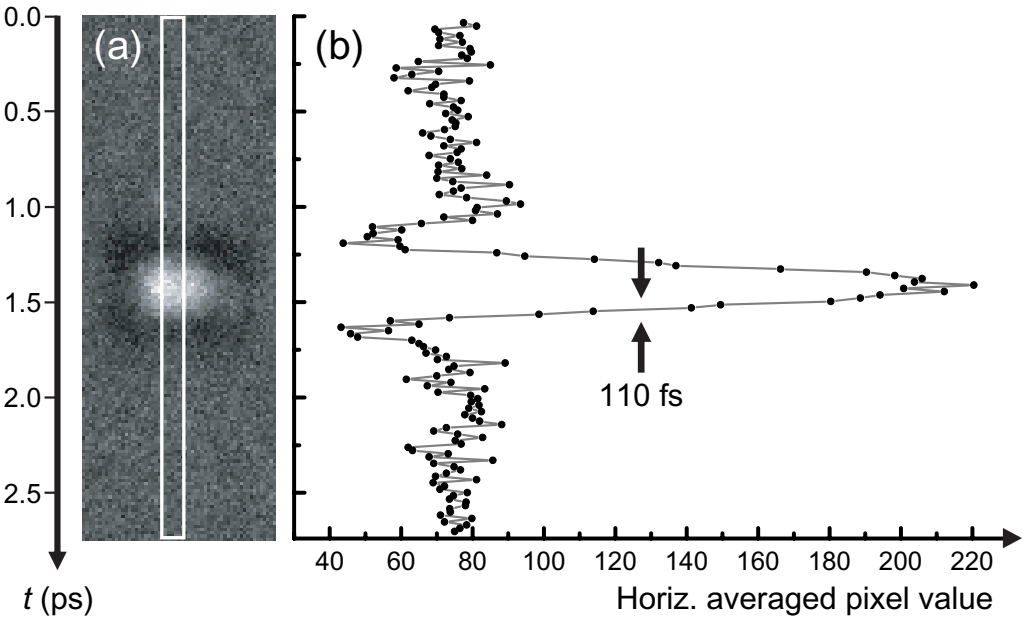

Figure 2. (a) Single-shot reflectivity change: areas where the x-ray pulse hits the substrate before the visible pulse is reflected appear brighter. The time axis t is shown on the left. The time zero is arbitrarily set to the top of the image. (b) Average signal of pixels within the ROI marked in (a). One pixel corresponds to 17 fs. The rise-time of 110 fs is equivalent to the pulse duration of the optical laser. The inflection point is used as the x-ray arrival-time marker.

3. Charge-states of Xe under moderate x-ray FLASH irradiance

Photoionization of Xe (ground state electron configuration [Kr] $4d^{10}5s^25p^6$) at 92 eV photon energy preferentially ionizes electrons from the 4d shell because of the $4d \rightarrow \epsilon f$ giant resonance, as is known from energy-resolved synchrotron studies [21]. The relaxation pathways of the created vacancies via single (A1) and double (A2) Auger decay involving several intermediate states were directly observed by detecting 4d and two Auger photoelectrons in coincidence [22]. Hence, one-photon photoionization of the 4d shell in Xe leads to Xe^{2+} and Xe^{3+} final states with two or three electron vacancies in the outer 5p shell, respectively. The time constants $\tau_{A1} = 6.0 \pm 0.7$ fs and $\tau_{A2} = 30.8 \pm 1.4$ fs were deduced from time-resolved experiments [2] in good agreement with energy-resolved measurements [21, 23].

Charge-states higher than Xe^{3+} cannot be created under low irradiance conditions with the x-ray photon energy near 92 eV because the threshold for Xe^{4+} production is approximately 105 eV. With increasing irradiance higher charged Xe states appear [24]. Even under our moderate irradiance conditions ($\sim 10^{12}$ W cm^{-2}) charged states of Xe^{4+} are already observed. Besides nonlinear excitation, an additional contribution from the third harmonic of the FLASH undulator at a photon energy near 3×92 eV $= 276$ eV has to be considered, the intensity of which is expected to be near to 1% of the fundamental [4]. The Xe^{3+} and Xe^{4+} ion yields unperturbed by the optical laser as a function of the x-ray pulse intensity (Xe^{2+} ion yield) are shown in figures 3(a) and (b), respectively. The Xe^{3+} ion yield shows a linear behavior and is fitted with $y = 0.71\,x$ (red solid line in figure 3(a)). The Xe^{4+} ion yield, by contrast, depends

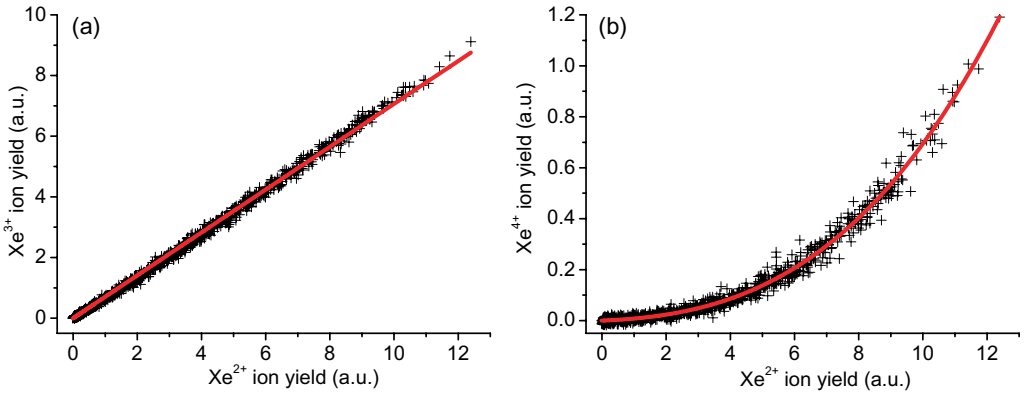

Figure 3. The single-shot Xe^{3+} (a) and Xe^{4+} (b) ion yield as a function of the x-ray pulse intensity (mapped by the Xe^{2+} ion yield) and the corresponding fit (red solid line). Data were collected using 1004 subsequent shots of the free-electron laser.

nonlinearly on the x-ray intensity and is best fitted with a third order polynomial function (red solid line in figure 3(b)):

$$y = (3.9x^3 + 25.8x^2 + 50.42x) \times 10^{-4}$$

indicating that linear (probably, FLASH's third harmonic), as well as nonlinear (most probably two-photon), processes are involved in the Xe^{4+} formation. Possible pathways for the latter case are $4d^{-2} \rightarrow 4d^{-1}5p^{-2} \rightarrow 5p^{-4}$ and $4d^{-1} \rightarrow 5p^{-2}$, $4d^{-1}5p^{-2} \rightarrow 5p^{-4}$.

The data for figure 3 were collected within 1004 subsequent pulses, demonstrating that shot-to-shot intensity fluctuations of FLASH pulses can be very strong. This will introduce a substantial noise into the time-dependent pump–probe spectra and complicate data analysis. The problem can be eliminated by a long acquisition time and by sorting the data according to the x-ray pulse intensity into groups with high, moderate and low Xe^{2+} ion yield. A substantial improvement is achieved by this approach, allowing detection of the transient Xe^{5+} signal (see below), which could not be resolved in the non-sorted data set.

4. Exploiting the intrinsic temporal resolution of FLASH with an ion-charge-state chronoscopy experiment

To assess the maximum possible temporal resolution of pump–probe experiments at FLASH, the transient Xe^{3+} and Xe^{4+} ion yields are considered. The energy levels and transitions in Xe ions relevant to this study are shown in figure 4(a), as composed from [2, 25]. The vacancy in the 4d shell created by the x-ray pump pulse decays to Xe^{2+} in a $5p^{-2}$ configuration and via intermediate states, mainly $5s^{-1}$ $5p^{-2}$ ns(np), to Xe^{3+} in a $5p^{-3}$ configuration (gray short-dashed arrows). Some of these intermediate states, presumably $5s^{-1}5p^{-2}6p$ as well as $5p^{-3}$nl (not shown in figure 4(a)), are below the threshold for Xe^{3+}. They are long lived compared to the timescale of the experiment. The laser pulse (blue solid arrow) can ionize these states, inducing an additional time-dependent increase in the Xe^{3+} ion yield.

The transient contribution to the Xe^{4+} ion yield arises from a series of shake-up satellites $4d^{-1}5p^{-1}$np populated by the x-ray pulse. These Xe^{1+} highly excited states decay via

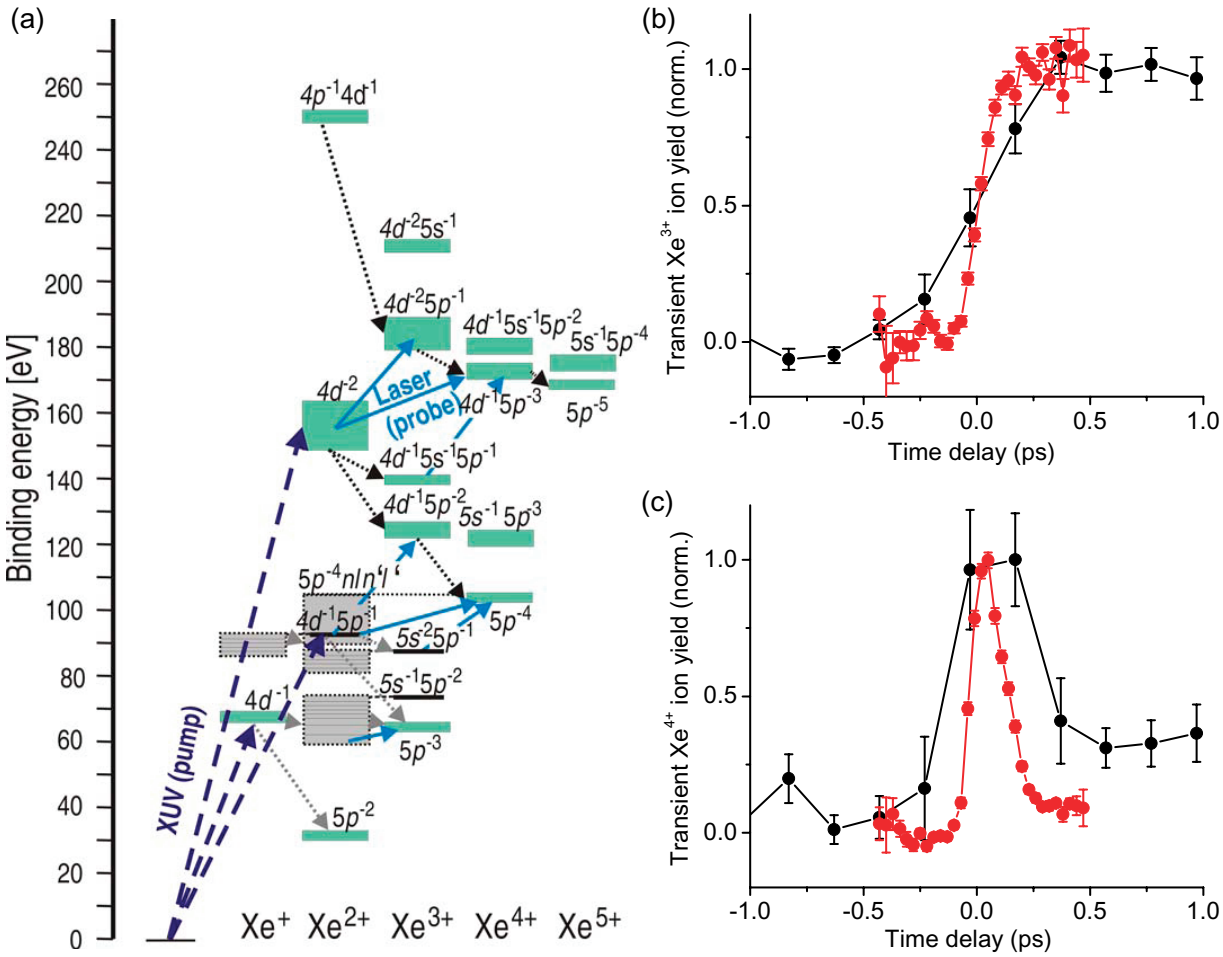

Figure 4. (a) Transitions in Xe, excited by x-ray and probed by visible laser pulses (from [2, 25]). (b) Transient Xe^{3+} and (c) Xe^{4+} ion yields, background subtracted and normalized, as a function of the time delay between x-ray pump and visible probe pulses. Black circles are a delay scan without correction of the x-ray pulse jitter. Jitter compensation with the x-ray/visible cross-correlator results in a dramatic improvement of the temporal resolution (red circles). Error bars are standard errors of the mean.

single $4d^{-1}5p^{-1}np \rightarrow 5s^{-2}5p^{-1}nl$ and double $4d^{-1}5p^{-1}np \rightarrow 5p^{-4}nln'l' \rightarrow 5p^{-3}$ Auger decay channels. In the latter case, short-lived $5p^{-4}nln'l'$ intermediate states are involved. Again, these intermediate states can be ionized by the laser probe pulse, leading to the transient Xe^{4+} signal [2]. Additionally, the $4d^{-1}5p^{-1}$ configuration can be directly photoionized by the x-ray pulse. This state can be further ionized by an optical laser to $4d^{-1}5p^{-2}$, initializing the $4d^{-1}5p^{-2} \rightarrow 5p^{-4}$ decay channel, before it decays to Xe^{3+} in a $5p^{-3}$ configuration.

An averaged Xe^{3+} and Xe^{4+} ion yield as a function of the time delay between x-ray (pump) and visible laser (probe) pulses is shown in figures 4(b) and (c), respectively. Transient changes of the ion yields are observed within a broad time window of about 0.7 ps for both signals (black circles). The data were collected by scanning an optical delay line with 10 second acquisition time per 200 fs step (about 50 ion traces per step), without any compensation for arrival time

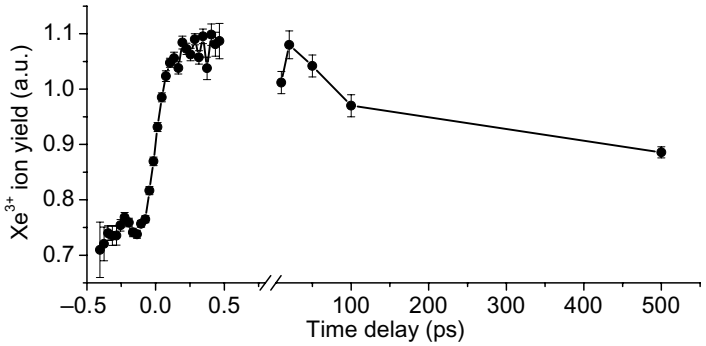

Figure 5. Transient Xe^{3+} ion yield in arbitrary units (a.u.) composed of data sets on two timescales. For delay times up to 0.5 ps, data are arranged subsequently within 30 fs time bins using arrival time information from the x-ray/visible cross-correlator. Up to delay times 10 ps the data are averaged without sorting. Error bars are standard errors of the mean.

fluctuations. Within a second run (red circles) 7514 ion traces were collected at a fixed optical delay stage position. For 4024 traces arrival times were delivered by the x-ray/visible cross-correlator. The data were arranged accordingly in 30 fs time bins. Ion traces with particularly low and high Xe^{2+} ion yield (x-ray pulse energy below 0.5 μJ and higher than 3 μJ) were excluded. Each data point in figures 4(b) and (c) is averaged over 9 to 40 shots for the delay scan data and over 10 to 44 shots for the data acquired at a fixed delay stage position. The time window, where transient changes in the ion yield are observed, is noticeably contracted to about 0.2 ps, demonstrating an essential improvement in the temporal resolution of the transient signal.

The shape of the transient profiles is characterized by the lifetime of the 4d hole (τ_{A1}) and of the involved intermediate states, respectively. No decrease of the laser-enhanced Xe^{3+} ion yield up to the maximum delay time of 300 fs was observed previously [2], this being indicative of a very long lifetime of the intermediate states. Our characterization of these long-lived excited states reveals that the transient ion yield of Xe^{3+} is reduced by approximately a factor of two after 500 ps (figure 5). This cannot be an artefact due to the limited stay of the Xe^{2+} ions in the laser focus, estimated to be 5 to 8 ns.

5. Discussion of deduced time constants

The temporal resolution and the lifetimes of the intermediate states are deduced from fitting of the transient profiles. The profile of the transient signal is generally described by a convolution integral over an instrument response function $R(t)$ and a response from the sample $S(t)$

$$I(t) = \int R(t - t')S(t')\,\mathrm{d}t',$$

$R(t)$ can be approximated by a Gaussian with a width σ

$$R(t) = B_1 \exp\left(-\frac{t^2}{2\sigma^2}\right), \quad \sigma = \sqrt{\sigma_{\mathrm{Laser}}^2 + \sigma_{\mathrm{Xray}}^2 + \sigma_{\mathrm{res}}^2},$$

where: $\sigma_{\mathrm{Laser}} = 51$ fs, $\sigma_{\mathrm{Xray}} = 15$ fs [12] and σ_{res} are Gaussian widths of the laser pulse, the x-ray pulse and a residual timing uncertainty, respectively. If a temporal jitter of the x-ray pulse is completely compensated for by the x-ray/visible cross-correlator, σ is expected to be 53 fs.

By instantaneous photoionization followed by an ultrafast Auger decay ($\tau_{A1} \ll \sigma$) the intermediate state is immediately populated and decays exponentially with the time constant τ

$$S(t) = B_2 \exp\left(-\frac{t}{\tau}\right).$$

Evaluating the convolution integral, fit functions for the transient Xe^{3+} and Xe^{4+} ion yields are obtained

$$S_{Xe^{3+}}(t) = B_{Xe^{3+}} \cdot \left(1 + \mathrm{erf}\left(\frac{t}{\sqrt{2}\sigma}\right)\right)$$

by assuming for Xe^{3+} $\tau \to \infty$ on the timescale considered here,

$$S_{Xe^{4+}}(t) = B_{Xe^{4+}} \exp\left(\frac{\sigma^2}{2\tau^2} - \frac{t}{\tau}\right)\left(1 - \mathrm{erf}\left(\frac{\sigma^2 - t\tau}{\sqrt{2}\sigma\tau}\right)\right),$$

where erf is the error function and B is an amplitude. The fitting routine is based on the Matlab R2008b Optimization Toolbox 4.1.

An example of single-shot data (black open circles) and the corresponding fit curve (red solid line) for Xe^{3+} and Xe^{4+} ion yields is shown in figures 6(a) and (b), respectively. The fit parameter $\sigma = 53 \pm 11$ fs (standard deviation (s.d.)) is in good correspondence with the expected value of 53 fs, demonstrating the efficient compensation for the temporal jitter by the x-ray/visible cross-correlator. The decay time $\tau = 103 \pm 26$ fs extracted from the Xe^{4+} transient ion yield curve is considerably longer than the value of $\tau_{A2} = 30.8 \pm 1.4$ fs found in [2].

A possible physical cause for this obvious discrepancy from the previous result could be the participation of additional long-lived intermediate electronic states, owing to the 400 nm probe wavelength (800 nm in [2]), and contributions from nonlinear excitation of the Xe 4d core level (unavailable in [2]). However, since the experimentally observed ion-charge state does not carry information about its energetic origin, it is not clear which state could exhibit a slower secondary decay and why this state would preferentially be probed with 400 nm radiation. A more technical reason for the discrepancy could be an asymmetric temporal profile of the 400 nm laser pulse which would effectively pretend an exponential decay if its trailing edge happened to be shallower than the rising edge. In our experiment, we could confirm a symmetrical profile only for the 800 nm fundamental laser. The—technically much more challenging—temporal characterization of its second harmonic at 400 nm was not possible. Although the simulation of the second harmonic generation in a BBO crystal did not indicate this, we cannot preclude a residual spectral phase of odd order that would lead to an asymmetrical profile. It is evident that extraction of unambiguous temporal information about the Auger processes investigated here requires considerably shorter and better controlled light pulses.

6. Double ionization of Xe 4d core level

As mentioned above, a common analysis of the data in groups of increasing Xe^{2+} ion yields substantially improves the signal-to-noise ratio. In a group with very high Xe^{2+} ion yield

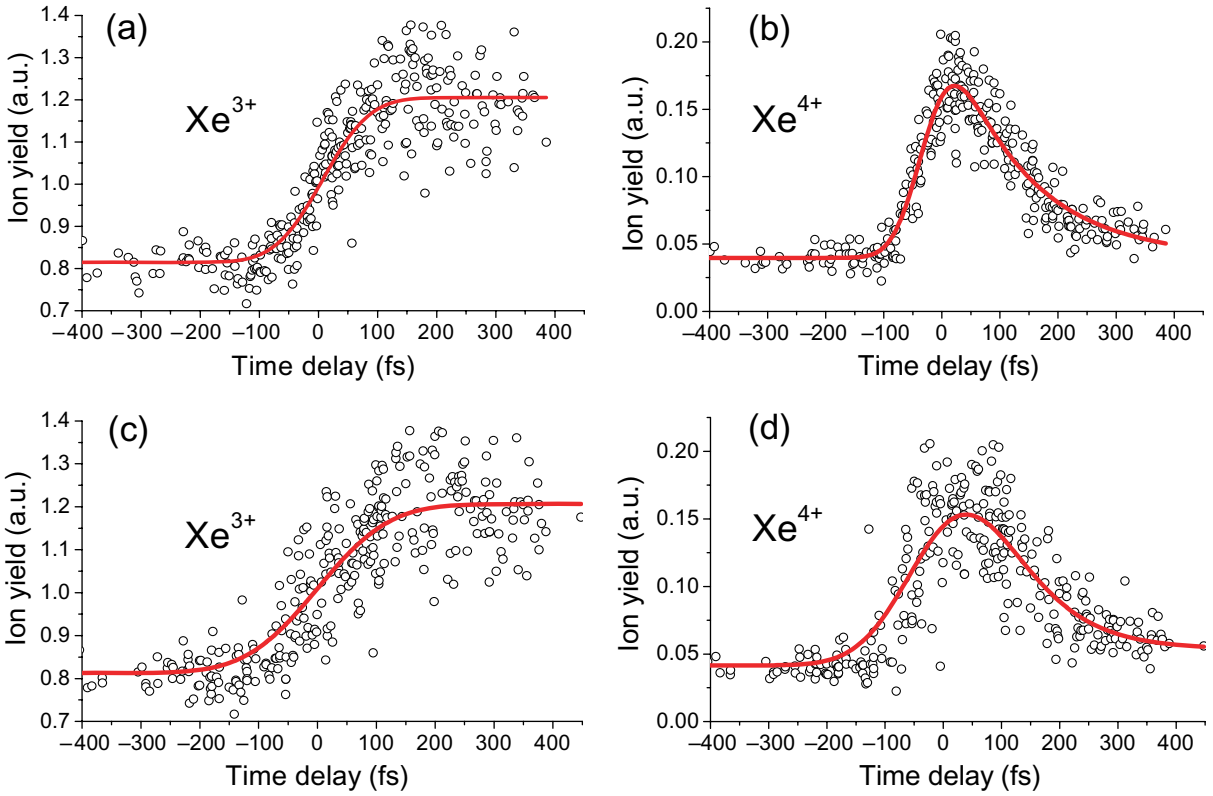

Figure 6. (a) and (b) Black open circles depict, respectively, single-shot Xe^{3+} and Xe^{4+} ion yields as a function of the delay. The data are sorted according to the x-ray arrival time measured by the x-ray/visible cross-correlator. The red solid curve represents fit results. (c) and (d) are the same data set as (a) and (b), but data are sorted according to the electron bunch arrival time measured with EOS.

(x-ray pulse energy higher than 3 μJ) Xe^{5+} ions were observed for the first time (figure 7). The transient profile of the Xe^{5+} ion yield is fitted with the same model function as Xe^{4+} and a decay time of $\tau = 81 \pm 36$ fs is deduced (the error given is a statistical one, see the discussion of systematic errors in section 5). The threshold for Xe^{5+} formation is about 168 eV, indicating that only excitation by the FLASH's third harmonic and/or two-photon ionization can be responsible for this process. V. Jonauskas *et al* [25] describe the most intense de-excitation pathways following 3d ionization (black dashed arrows in figure 4(a)) ending in the Xe $5p^{-4}$ and $5p^{-5}$ configuration. The non-vanishing Xe^{4+} ion yield as well as its nonlinear dependence on the Xe^{2+} ion yield in the laser unperturbed spectra (figure 3(b)) indicate a $4d^{-2} \rightarrow 5p^{-4}$ decay channel. An optical laser can further ionize the $4d^{-2}$ state and the $4d^{-1}5s^{-1}5p^{-1}$ intermediate state, activating the $4p^{-1}4d^{-1} \rightarrow 5p^{-5}$ decay channel.

Xe ionic states were extensively studied as a function of the intensity of FLASH pulses up to 10^{16} W cm^{-2} [24, 26 and references therein]. The degree of nonlinear photoionization was found to be significantly higher in Xe than in the rare gases argon, neon and krypton [26]; the $4d \rightarrow \epsilon f$ giant resonance was held responsible for this behavior. For ion charge states up to Xe^{6+} a stepwise multi-photon absorption attended by a subsequent Auger decay between single steps was proposed as a possible mechanism [24]. Our observation of a transient Xe^{5+}

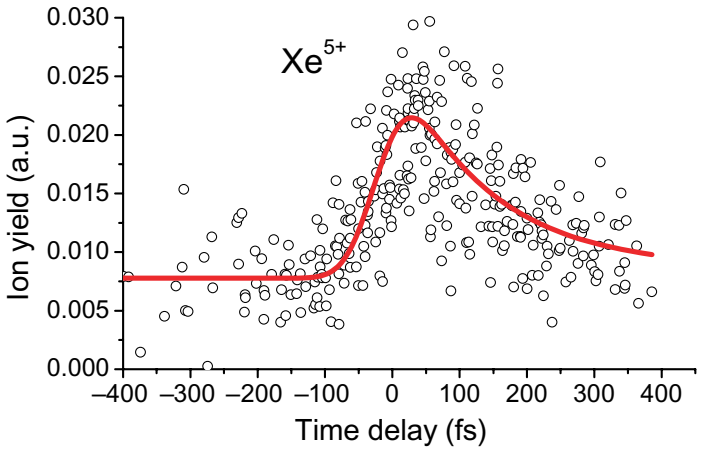

Figure 7. Single-shot Xe^{5+} ion yield as a function of the delay time (black open circles). Data are sorted according to the x-ray arrival time measured by the x-ray/visible cross-correlator. The red solid curve represents fit results.

ion yield requires, however, the formation of short-lived Xe $4d^{-2}$ states in the absorption process. Hence, these results indicate that already at lower intensity the 4d shell can be double-ionized by two-photon absorption, before a single vacancy is refilled by Auger decay.

7. Photon–photon versus photon–electron cross-correlation

With the EOS setup available at FLASH [27], the electron bunch arrival time can be measured simultaneously to the x-ray pulse arrival time at the experimental end-station. Ascribing both arrival times to the same pump–probe data set, the temporal resolution of both approaches can be directly compared. Runs with a correlation coefficient of 0.98 are selected for further analysis. Figures 6(c) and (d) show the same pump–probe data set as figures 6(a) and (b), but the time axis corresponds to the electron bunch arrival time measured by EOS, instead of the x-ray pulse arrival time measured at the experimental end-station. Applying the same fitting algorithm as discussed in the previous section, σ is deduced to be 75 ± 16 fs (s.d.). Comparing this value with the expected one, we estimate a remaining uncertainty in the temporal resolution of $\sigma_{\mathrm{res}} = 55$ fs or 130 fs FWHM.

The statistical nature of the SASE process, together with any possible jitter sources associated with the long x-ray beam transport to the experiment location, is not compensated for by EOS. An additional origin of jitter can be connected with the optical laser transport to the location of the EOS device in the FLASH tunnel. The optical laser undergoes pulse broadening within the 153 m long optical fiber. Moreover, the pulse arrival time can drift due to thermal length changes and microphonic pick-up. Thus, sophisticated pulse recompression and fiber feedback schemes have to be realized [27]. For some runs a long-term drift in the optical laser pulse arrival time is observed as a linear offset in correlation plots of the electron bunch arrival times via x-ray pulse arrival times (data not shown). Such runs were excluded from comparison.

8. Summary and outlook

Electron relaxation in Xe atoms was initiated by excitation of the 4d-shell with 92 eV soft x-ray pulses of the free-electron-laser FLASH. The transient population and depopulation of intermediate states was probed with intense 400 nm laser pulses, promoting Rydberg electrons into the continuum, thus leaving ions with up to fivefold positive charge. Arrival time fluctuations between soft x-ray and laser pulses were efficiently compensated for using a simultaneously operated optical cross-correlator for the tagging of individual shots with measured time delays. Ion-charge-state chronoscopy of Xe^{3+} and Xe^{4+} ionic states was used to evaluate the corresponding improvement in the timing of x-ray-pump/laser-probe experiments. With an instrumental response time of approximately 120 fs (FWHM) the temporal resolution is now clearly dominated by the laser pulse duration. Using shorter laser pulses the precision of the tagging technique utilized in this work has the potential to push the temporal resolution towards the intrinsic limit dictated by the soft x-ray pulse duration of 35 fs FWHM [12]. A direct comparison with an electron/laser cross-correlation based on EOS suggests that the optical–optical correlation yields superior precision, if a timing jitter below 50 fs rms is required.

So far, the achieved resolution, restricted by the optical laser pulse duration, has not permitted a precise determination of time constants for the Xe NOO Auger decay. It will, however, become sufficient for following the dynamics of processes evolving on a timescale of a few tens of femtoseconds, e.g. secondary steps in an Auger cascade [2], or interatomic Coulomb decay [28]. As an observation of the latter requires the preparation of very dilute gaseous targets, only the high flux of accelerator-based soft x-ray sources makes such studies feasible. The significance of high soft x-ray intensities is underlined by the observation of an Xe^{5+} ionic state which we assign to a double-ionization of the Xe 4d core level, the transient decay of which could be followed. Time-resolved nonlinear x-ray physics is a promising objective for existing and upcoming accelerator-based x-ray sources. In order to fully resolve the dynamics, the temporal resolution still has to be optimized. The tagging technique utilized in this work has contributed a substantial improvement and will further aid this process.

Acknowledgments

This work was supported by the Bundesministerium für Bildung and Forschung (BMBF 05-KS4PB1/0). We thank the scientific and technical team for operating the machine and for support at the beamline of FLASH.

References

[1] Drescher M *et al* 2002 *Nature* **419** 803
[2] Uiberacker M *et al* 2007 *Nature* **446** 627
[3] Uphues Th *et al* 2008 *New J. Phys.* **10** 025009
[4] Tiedke K *et al* 2009 *New J. Phys.* **11 0**23029
[5] Bocchetta C J *et al* 2007 *FERMI@Elettra Conceptual Design Report* ST/F-TN-07/12
[6] Arthur J *et al* 2002 *Conceptual Design Report* No. SLAC-R593 (Stanford). See also http://ssrl.slac.stanford.edu/lcls/cdr)
[7] Shintake T *et al* 2008 *Nat. Photonics* **2** 555

[8] Altarelli M *et al* (ed) 2006 *Technical Design Report* No. DESY 2006-097 (DESY). Preprint at http://xfel.desy.de
[9] Cunovic S *et al* 2007 *Appl. Phys. Lett.* **90** 121112
[10] Radcliffe P *et al* 2007 *Appl. Phys. Lett.* **90** 131108
[11] Pietzsch A *et al* 2008 *New J. Phys.* **10** 033004
[12] Frühling U *et al* 2009 *Nat. Photon.* **3** 523
[13] Mitzner R *et al* 2009 *Phys. Rev.* A **80** 025402
[14] Winter A 2008 *PhD thesis* http://www.physnet.uni-hamburg.de/services/fachinfo/___Volltexte/Axel___Winter/Axel___Winter.pdf
[15] Lambert G *et al* 2008 *Nature Phys.* **4** 296
[16] Azima A *et al* 2008 *Proc. EPAC 2008* (Genoa, 23–7 June, 2008) pp 127–9
[17] Gensch M *et al* 2008 *Infrared Phys. Technol.* **51** 423
[18] Fritz D M *et al* 2007 *Science* **315** 633
[19] Cavalieri A L *et al* 2005 *Phys. Rev. Lett.* **94** 114801
[20] Maltezopoulos Th *et al* 2008 *New J. Phys.* **10** 033026
[21] Holland D M P *et al* 1979 *J. Phys. B: At. Mol. Phys.* **12** 2465
[22] Penet F *et al* 2005 *Phys. Rev. Lett.* **95** 083002
[23] Jurvansuu M, Kivimäki A and Aksela S 2001 *Phys. Rev.* A **64** 012502
[24] Sorokin A A *et al* 2007 *Phys. Rev. Lett.* **99** 213002
[25] Jonauskas V *et al* 2003 *J. Phys. B: At. Mol. Phys.* **36** 4403
[26] Richter M *et al* 2009 *Phys. Rev. Lett.* **102** 163002
[27] Azima A *et al* 2009 *Appl. Phys. Lett.* **94** 144102
[28] Santra R, Zobeley J and Cederbaum L S 2001 *Phys. Rev.* B **64** 245104